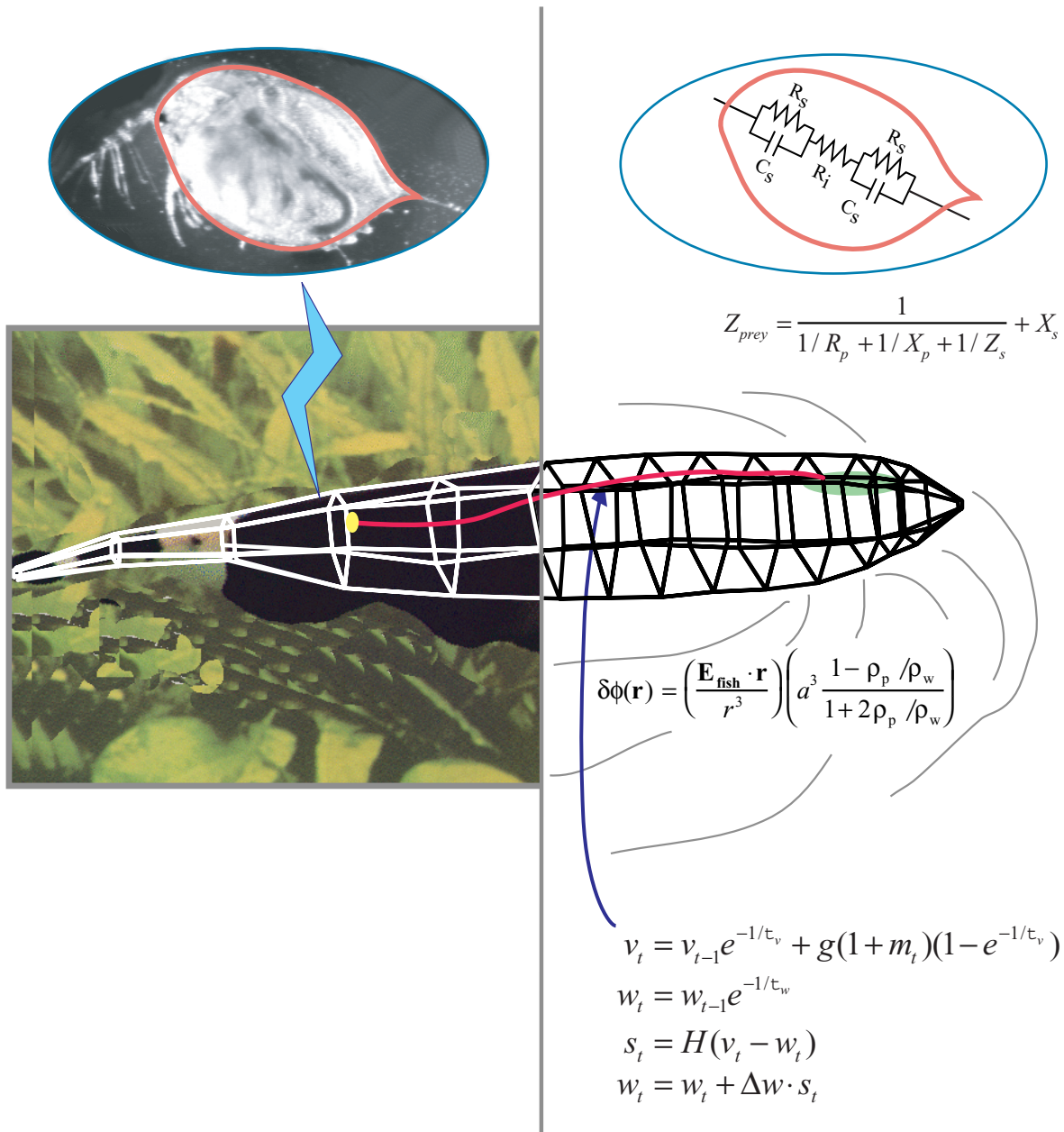


# The computational neuroethology of weakly electric fish body modeling, motion analysis, and sensory signal estimation



UNIVERSITY OF ILLINOIS AT URBANA-CHAMPAIGN  
THE GRADUATE COLLEGE

MARCH 2001

(date)

WE HEREBY RECOMMEND THAT THE THESIS BY

MALCOLM ANGUS MACIVER

ENTITLED THE COMPUTATIONAL NEUROETHOLOGY OF WEAKLY ELECTRIC FISH: BODY

MODELING, MOTION ANALYSIS, AND SENSORY SIGNAL ESTIMATION

BE ACCEPTED IN PARTIAL FULFILLMENT OF THE REQUIREMENTS FOR

THE DEGREE OF DOCTOR OF PHILOSOPHY

*Mark E. Nelson*

Dr. Mark E. Nelson

Director of Thesis Research

*Gene E. Robinson*

Dr. Gene E. Robinson

Head of Department

Committee on Final Examination†

*Mark E. Nelson*

Dr. Mark E. Nelson

Chairperson

*Thomas J. Anastasio*

Dr. Thomas J. Anastasio

*Neal J. Cohen*

Dr. Neal J. Cohen

*Albert S. Feng*

Dr. Albert Feng

*Joseph G. Malpeli*

Dr. Joseph G. Malpeli

† Required for doctor's degree but not for master's.

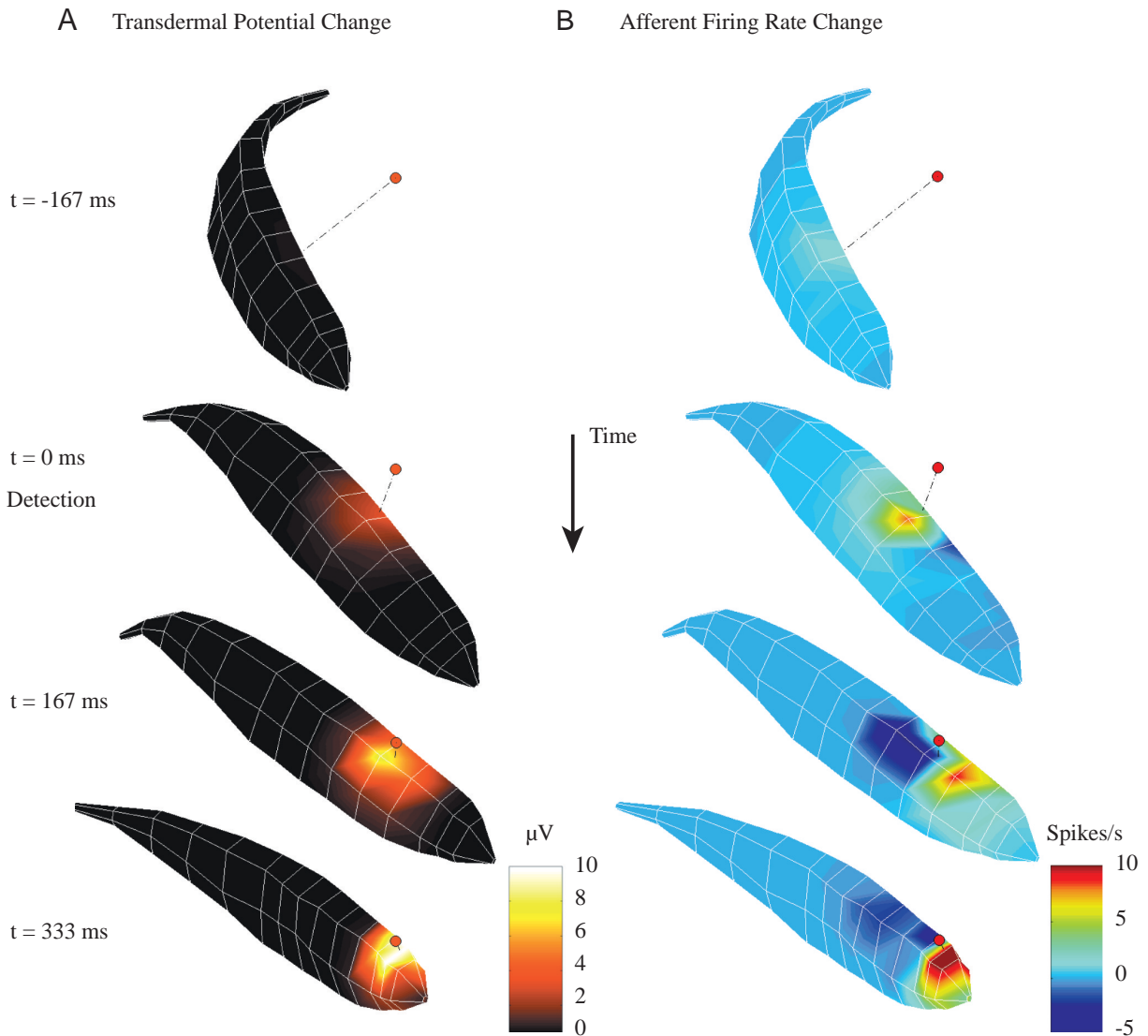


**Figure 3.7** False color maps of reconstructed electrosensory images generated from model-based tracking of a single prey capture sequence. The weakly electric fish (*Apteronotus albifrons*) is able to detect prey in the dark by sensing small perturbations in a self-generated electric field. Each column shows 'snapshots' of the polygonal fish model at four different times in the prey capture sequence. The left-hand column (A) shows the voltage change across the skin (transdermal potential) induced by the prey. The right-hand column (B) shows the corresponding change in electrosensory afferent firing rate due to the voltage perturbations shown in (A). The prey (*Daphnia magna*) is shown as a red dot; the dashed line represents the shortest distance between the fish and the prey. Modified from Nelson & MacIver, 1999.

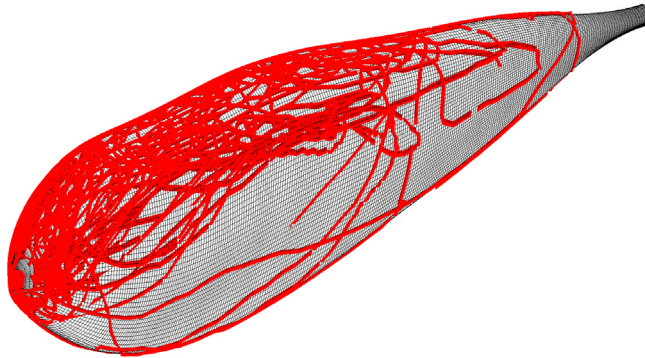


**Figure 4.7** Prey tracks on fish surface. Lines connect the closest points on the fish surface to the prey over the course of a prey capture sequence ( $N = 116$ ). These tracks are concentrated on the dorsal aspect of the fish, where there is a higher concentration of receptors (Fig. 5.3).

#### **4.4.4 Distribution of prey “tracks” on fish surface**

The temporal variation in location of the closest point on the surface of the fish to the prey, which will be referred to as the prey “track” for simplicity, is illustrated in Fig. 4.7 for all trials. Both prior to and following detection the location of the prey track is constrained largely to the dorsal aspect. In part, this is the result of active positioning of the dorsum with respect to the prey through rolling behavior (see Section 4.4.6 and Fig. 4.10 below).

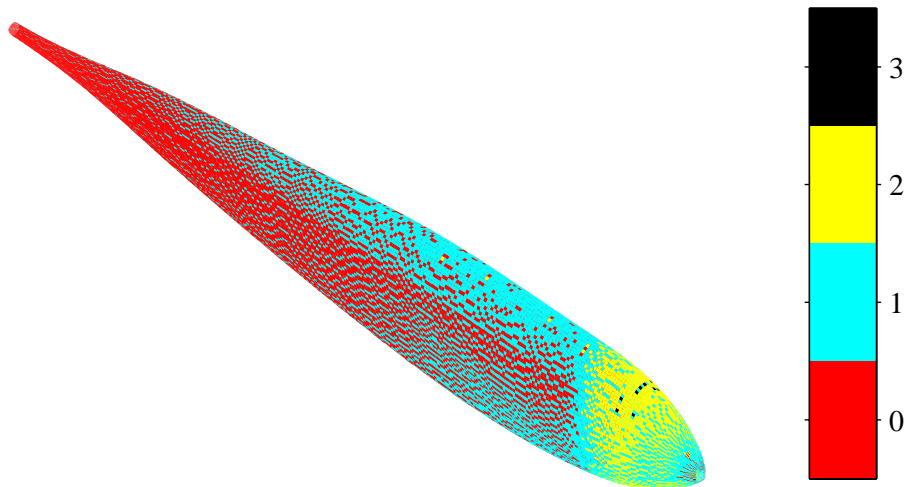


**Figure 5.1** Tuberous receptor count by surface model facet. While there is an order of magnitude increase in the density of receptors at the head compared to the trunk, the number on each facet stays close to between 0 and 2 throughout. The ribbon and pectoral fins do not possess electroreceptors.

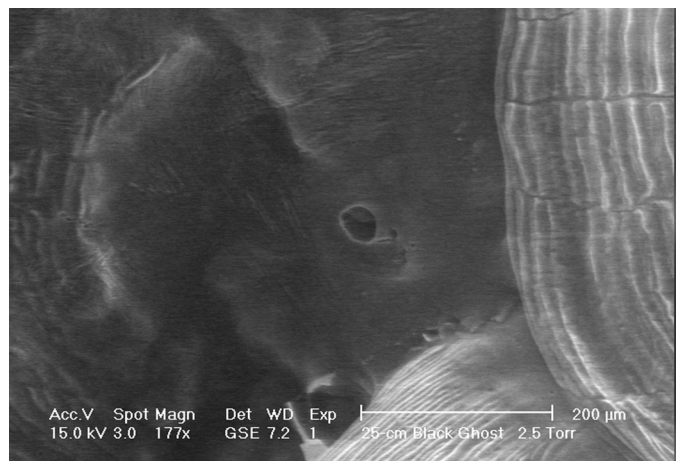


**Figure 5.2** Environmental scanning electron micrograph of tuberous receptor pore. The pore is located on the rostral edge of the fish scale (the anterior of the fish is to the right), as observed by Suga (1967).

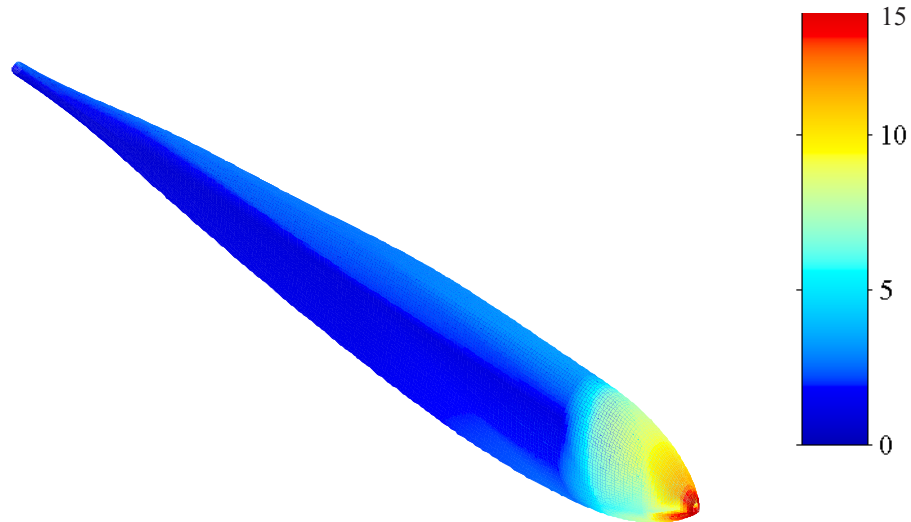


**Figure 5.3** Tuberous receptor density on the surface of *A. albifrons*, reconstructed from data presented in Carr et al. (1982). There is an order of magnitude increase in density rostral of the operculum, a region sometimes referred to as the electrosensory “fovea”. There is also an increase in the density at the dorsal and ventral edges of the body. The ribbon and pectoral fins do not possess electroreceptors.

### 5.3.3 Estimating the electric field at the prey

The analytic model we use for computing the input for each electroreceptor requires the magnitude and direction of the electric field vector at the location of the prey. The electric field around a fish varies with a number of factors, including fish size, conductivity of the water, deformation of the body such as tail bending, and objects in the environment. We will make several simplifying assumptions in light of these sources of variation. First, we will use detailed measurements of the electric field around a 10 cm *A. albifrons* obtained from other researchers (B. Rasnow, C. Assad, P. Stoddard, 1993 unpublished measurements, collected as detailed in Rasnow and Bower 1996). The magnitude of the field is shown in Fig. 5.4. The length of the fish that was mapped was similar to the 13 cm mean length of the subjects in this study. Second, we will neglect the effects of body deformation, and utilize measurements of the field around a straight fish. Measurements of afferent activity indicate that large amplitude ( $\pm 45^\circ$ ) tail

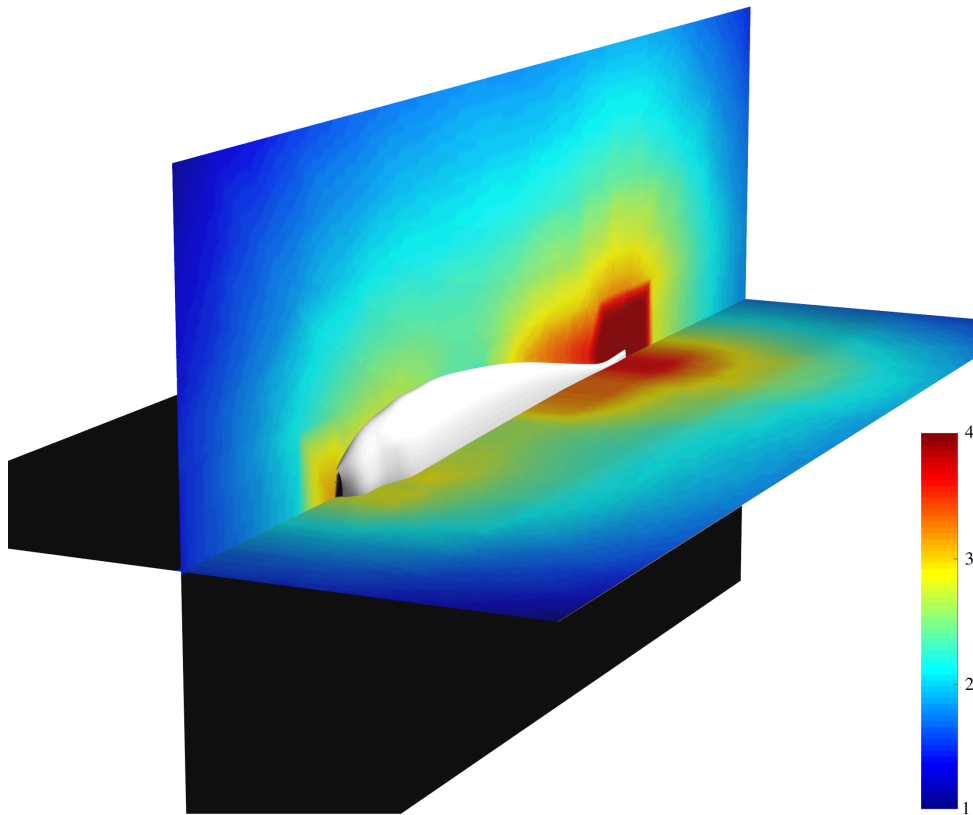
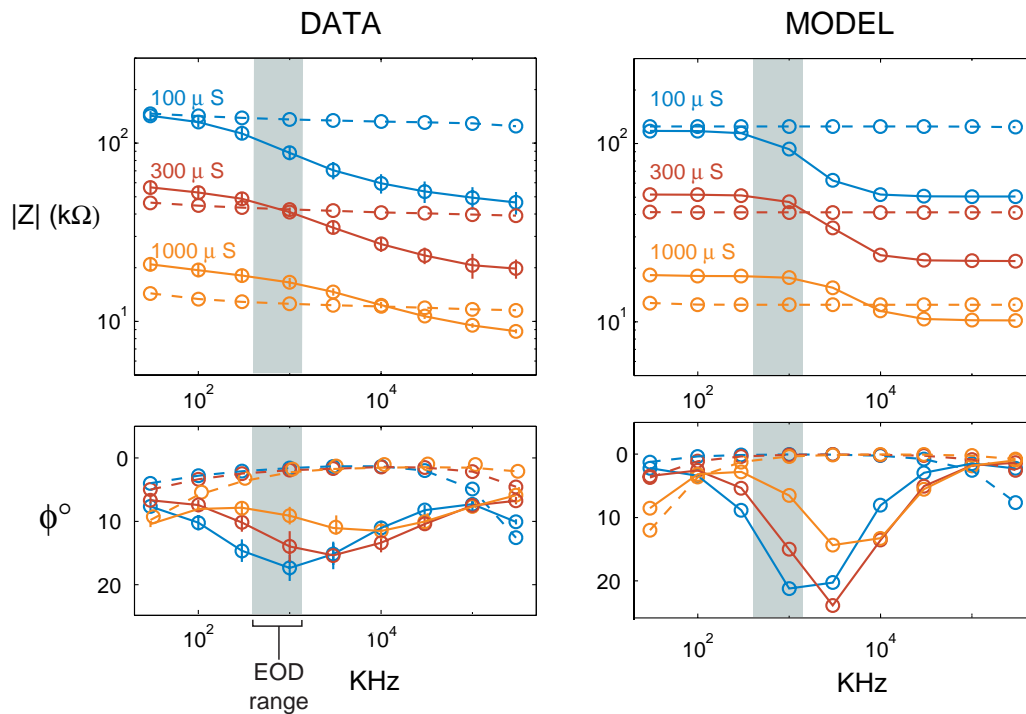


**Figure 5.4** The magnitude of the dorsal and median plane electric field vectors for a 9.8 cm *A. albifrons* in  $210 \mu\text{S} \cdot \text{cm}^{-1}$  water,  $\log \mu\text{V}$  of the RMS value over one electric organ discharge cycle (B. Rasnow, C. Assad, and P. Stoddard, 1993 unpublished measurements collected as detailed in Rasnow and Bower 1996). A surface model of the mapped fish is also shown.

## 5.4 Results

### 5.4.1 Prey impedance

The results of our measurements of the impedance of live *Daphnia magna*, the first such measurements of a live small animal we know of, are shown in Fig. 5.6.



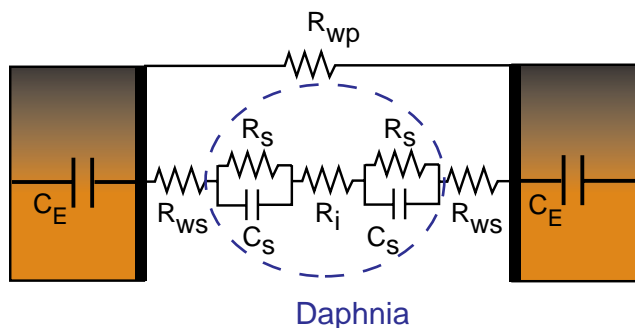
**Figure 5.6** Measured and modeled impedance of live *Daphnia* at three water conductivities and nine test frequencies. These three conductivities bracket the natural range found in the fish’s habitat. Dashed lines are the impedance of the cell without *Daphnia* (volume replaced with water of test conductivity); solid lines are the impedance with live *Daphnia* in the test chamber. The light green bands show the range of electric organ discharge frequencies for individual *Apteronotus*.

Fig. 5.6 shows both the magnitude of the impedance and its phase as a function of test frequency. The impedance of the test cell containing only the test solution is shown as dashed lines, while the test cell with *Daphnia* is shown with solid lines. We observe that the conductiv-

1000  $\mu\text{S}$ , the highest value used in these measurements, he found that fish were unable to make discriminations on the basis of capacitance; he hypothesized that this was due to a reduction in EOD amplitude at high conductivities (the EOD becomes effectively shorted at higher conductivity). We can see from Fig. 5.6 that the extent of the phase lag with *Daphnia* in the cell also decreases with increasing conductivity of the external milieu. This may thus contribute to the failure to discriminate capacitance in high conductivity water.

## 5.4.2 Prey electrical equivalent model

Several possible electrical equivalent circuits for the *Daphnia* in series with the electrode impedance and in parallel with the surrounding water were tested. We obtained the best match with empirical data with the configuration shown in Fig. 5.7.



**Figure 5.7** Electrical equivalent model of *Daphnia* and the test cell. Abbreviations:  $C_E$ , test cell electrode capacitance;  $R_{wp}$  resistance of parallel water path;  $R_{ws}$ , resistance of series water path;  $R_s$  resistance of one face of *Daphnia* exoskeleton;  $C_s$  the capacitance of one face of the exoskeleton;  $R_i$  the internal resistance of *Daphnia*.

The circuit is a resistor for the internal specific resistance for its body cavity ( $550\Omega \cdot \text{cm}$ ), in series with an identical leading and following circuit for the exoskeleton of the crustacean, consisting of a capacitor in parallel with a resistor ( $C_s = 1.2 \text{ nF}$ ,  $R_s = 230 \text{ k}\Omega$ ). Our best

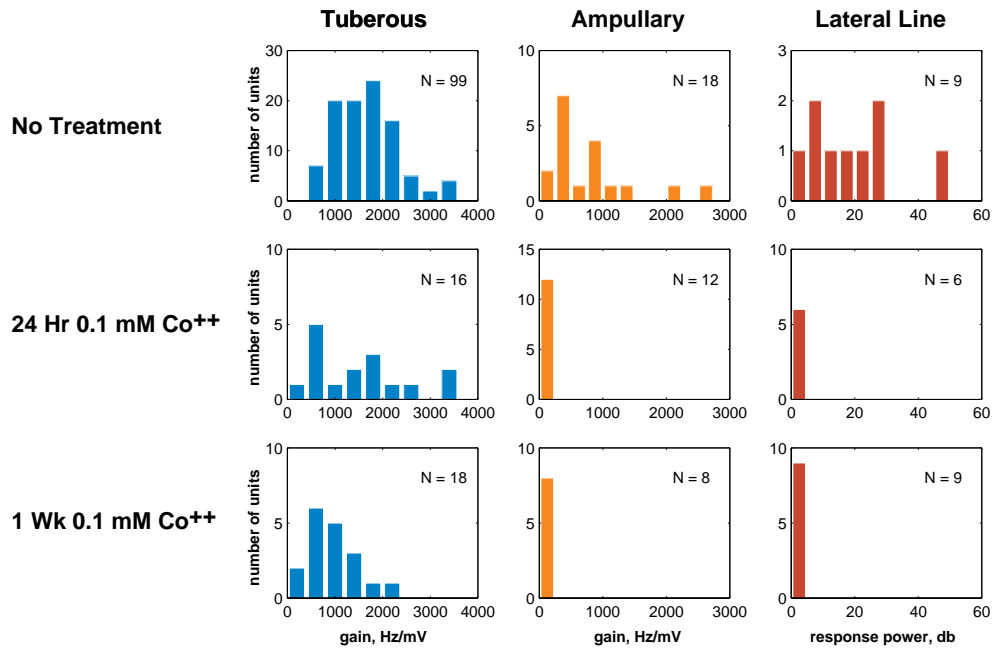


**Figure A.1** Effect of cobalt on response properties of electrosensory and mechanosensory afferents.

appears that there could be some decrease in tuberous gain after 1 week, but we need to collect more data to determine whether this effect is significant).

For the tuberous afferent control data, previously collected for other studies (Nelson et al., 1997), the gain was  $1,490 \pm 730$  Hz/mV; after 24 hours in 0.1 mM Co<sup>++</sup> week it was  $1,310 \pm 1,030$  Hz/mV. In comparison, the gain for untreated ampullary afferents was  $620 \pm 620$  Hz/mV, while after 24 hours in 0.1 mM Co<sup>++</sup> it dropped to  $3 \pm 1$  Hz/mV. Similarly, the uncalibrated response power for untreated mechanosensory units was  $17 \pm 14$  dB; after 24 hours in 0.1 mM Co<sup>++</sup> it dropped to 0 dB.

We have collected a limited amount of behavioral data with cobalt treated fish. Such fish showed no overt signs of systemic disruption at the low concentration of Co<sup>++</sup> used, in agreement with behavioral and physiological measures made by (Karlsen and Sand, 1987) in a dif-

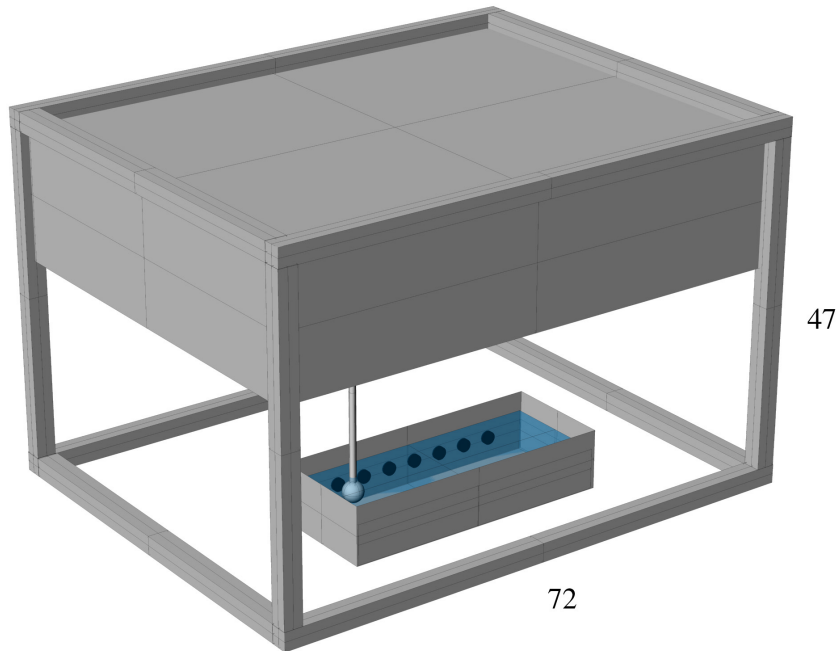


**Figure B.1** Schematic of the robotic workcell, test object, and sensors. Outer dimensions of the workcell are indicated in cm.

were moved past the electrosensory array using a three-axis robotic workcell (RW-18B, Arrick Robotics, Hurst, Texas, USA). The position and velocity of the target object was controlled using custom motion control software.

## B.4 Results

For a preliminary assessment of the system, we wanted to determine whether the signals from the sensor array were qualitatively similar to the transdermal potential modulations observed when a small object is placed near a weakly electric fish. Studies by Rasnow (1996) have shown that the electrosensory image of a small spherical object is spatially broad and weak for distant objects, and become sharper and stronger as the object approaches the fish. To